Mass Composition in Pre-Eruption Quiet Sun Filaments

Gary Kilper[1], Holly Gilbert[1,2], and David Alexander[1]

[1]Rice University, Physics and Astronomy Department, 6100 Main St, Houston, TX 77005; garyk1@gmail.com

[2]NASA Goddard Space Flight Center, Code 670, Greenbelt, MD 20771

ABSTRACT

Filament eruptions are extremely important phenomena due to their association with coronal mass ejections and their effects on space weather. Little is known about the filament mass and composition in the eruption process, since most of the related research has concentrated on the evolution and disruption of the magnetic field. Following up on our previous work, we present here an analysis of nineteen quiet Sun filament eruptions observed by MLSO in Hα and He I 10830 Å that has identified a compositional precursor common to all of these eruptions. There is a combined trend of an apparent increase in the homogenization of the filament mass composition, with concurrent increases in absorption in Hα and He I and in the level of activity, all starting at least one day prior to eruption. This finding suggests that a prolonged period of mass motions, compositional mixing, and possibly even extensive mass loading is occurring during the build up to these eruptions.

Subject headings: Sun: filaments — Sun: prominences — Sun: coronal mass ejections (CMEs)

1. Introduction

Filament eruptions are dramatic events in the solar atmosphere that expel material and magnetic field from the corona into the solar system. These eruptions have long been associated with coronal mass ejections (CMEs), which greatly affect the space weather at Earth and makes their understanding a key goal of solar physics. In particular, much effort has focused on explaining the wealth of recent observations that show the eruption process in many wavelengths (i.e. over a wide range of temperatures), leading to a better understanding of the eruption process and the establishment of several models related to the initiation of the eruption (e.g. Klimchuk 2001).

Filaments are structures embedded in the solar corona containing relatively dense, cool material that is confined by magnetic fields anchored in the photosphere and lying above a polarity inversion line (Tandberg-Hanssen 1995). The material is surrounded by a relative void (significantly less dense than the neighboring corona) and an overarching magnetic arcade. When viewed over the limb, the material and void are called a *prominence* and *cavity*, respectively. When observed against the solar disk, the material by itself is known as a *filament*, and the material together with the void is called a *filament channel*; note that filament channels can also lack material, consisting of only a void and magnetic arcade (e.g. see Gaizauskas et al. 1997). In general contexts, the terms prominence and filament can be used interchangeably.

The cool filament material is primarily composed of hydrogen and helium that is partially ionized, with the neutral atoms supported by interactions with the ions (Gilbert et al. 2002). Filaments and prominences are typically observed in near-infrared, optical, and extreme ultraviolet (EUV) spectral lines, while the cavity is seen in white light, EUV, and soft X-rays (SXR). *Quiet Sun filaments* and *active region filaments* are categorized by where they appear on the Sun and are generally considered to have very different

magnetic structures and formation processes. Quiet Sun filaments differ in the amount of activity they display throughout their lifetime, ranging from *quiescent*, when the filament displays little internal motion and has a stable size and shape, to *active*, when there are numerous small-scale motions and flows visible within the material and often a deepening in absorption (Martin 1998). Within this general context, we define *activation* in this study as a transition from a level near quiescent to fully active, which is observed to occur over a period of a few hours. *Eruptions* are an extreme in the observed behavior of filaments, with most starting with an initial slow rise, followed by a sharp change to a fast rise when they are high in the corona (Sterling & Moore 2001). Filament eruptions can be *full*, where all of the material is expelled, *partial*, where only some of the mass erupts, or *failed*, if the material resettles or falls back to the surface and does not result in a CME (Gilbert et al. 2007b). Note that several of the terms above have been used in the past with some ambiguity, and the definitions outlined here are meant to reduce possible confusion, at least within this paper.

Several past observational studies of filaments have centered on finding precursors to eruptions – such as the behavior during the build up, the rise speed and acceleration, and brightenings in high-temperature lines (e.g. SXR or EUV) – all with the goal of understanding the importance and timing of the relevant forces and energy release mechanisms (e.g. see Alexander 2006). Recent studies of flux emergence during the slow rise phase (Feynman & Ruzmaikin 2004; Sterling et al. 2007), its relation to CME initiation (Zhang et al. 2008), observations of heating both before (e.g. Cirigliano et al. 2004; Kucera & Landi 2006) and during eruptions (e.g. Engvold et al. 2001; Kucera & Landi 2008), and increases in the size of the cavity (Gibson et al. 2006) contribute pieces to the puzzle of determining the mechanism driving filament eruptions, and they help place the results of this study into context.

The present work is motivated by our initial findings from a detailed analysis that compared absorption between neutral hydrogen and helium lines in order to study the composition of quiet Sun filaments (Gilbert et al. 2007a; Kilper 2009). In that study, we found a significant trend, common to all five eruptions studied, of a compositional signature prior to the eruptions. Here, we apply an enhancement of the previous analytical method to a larger sample of eruptions, which is meant to test comprehensively and expand upon our initial findings. First, we describe the set of observations used and the analytical method (§ 2). We then outline the trends found and provide examples of two eruptions with contrasting properties (§ 3), and finally we interpret the results and discuss their ramifications (§ 4).

2. Observations and Analysis

The primary observations used in this paper were taken at the Mauna Loa Solar Observatory (MLSO), which observes the Sun in several optical and near-infrared wavelengths on a daily basis from 17:00 to 02:00 UT, depending on the duration of daytime and the weather conditions. The two instruments used here were installed as part of the Advanced Coronal Observing System (ACOS) in 1996-1997 and are operated by the High Altitude Observatory (HAO). The Polarimeter for Inner Coronal Studies (PICS) instrument has a Lyot filter centered at Hα 6563 Å and a removable occulter, and it observes the solar disk with a narrow 0.5 Å bandpass and a resolution of 2.9 $arcsec$ per pixel (the optical system is the same as P-MON in Fisher et al. 1981). Concurrent to the PICS observations, the Chromospheric Helium-I Imaging Photometer (CHIP) instrument observes He I 10830 Å with a tunable Lyot filter that has a bandpass of 1.4 Å and a resolution of 2.29 $arcsec$ per pixel (Kopp et al. 1997; Elmore et al. 1998). Note that the optical resolution of these instruments is approximately $7 - 8$ $arcsec$, which is equivalent to ~ 5 Mm on the Sun,

while the Doppler half-widths of the instruments' bandpasses are 11.4 km/s for Hα and 19.4 km/s for He I. The observations by both instruments are flat-fielded and calibrated at HAO, include the full solar disk, and are taken every three minutes for the years used in this study.

Out of many possible quiet Sun filament eruptions that were observed by MLSO between 2000 and 2006, thirty-eight were identified as good candidates due to the availability of sufficient observations. The nineteen eruptions selected for analysis have the most complete sets of observations in both the Hα and He I spectral lines for several days preceding the eruptions, and they also span a range of sizes, shapes, locations on the disk, and eruption types, which was done with the intention to fully test and broaden the impact of any results (see Table 1, below). For context information post-eruption, observations from the Solar and Heliospheric Observatory's (SOHO) Extreme Ultraviolet Telescope (EIT) and the Large Angle and Spectrometric Coronagraph (LASCO) were used to view the entire eruption and connect the resultant CMEs. Most of the measured CME parameters are obtained from the CDAW LASCO CME catalog, although it was necessary to measure one CME using the MLSO/Mk4 K-coronameter (on 2003 June 11).

The analysis used here is similar to the one described in Gilbert et al. (2007a), and for a treatment of the errors due to image misalignment, please refer to this earlier paper. The MLSO observations comprising each pair of Hα and He I being compared are as close together in time as possible, and are carefully aligned to ensure a proper measurement of the He/H absorption ratio. The alignment is done by shifting and then re-binning the pixels in the He I image to fit the Hα image. The pixels included as part of the filament must show a certain degree of absorption in Hα, which was determined by the threshold in trial runs that best selected the filament material without including too much random absorption in the background; Hα is used to identify the filament because in He I, active regions are also

seen in absorption, which would confuse the pixel selection process in filaments that are nearby. For each of the co-aligned pixels comprising the filament, the relative percentages of absorption from the average brightness values are calculated in the two lines and compared to yield the He/H absorption ratio (on a spatial scale of 2.9 $arcsec$):

$$(He/H \; absorption \; ratio)_{pixel} = \frac{1 - (He_{pixel}/He_{avg})}{1 - (H\alpha_{pixel}/H\alpha_{avg})} \; ,$$

where He_{pixel} and $H\alpha_{pixel}$ are the numerical values of that pixel in the two lines, and He_{avg} and $H\alpha_{avg}$ are average pixel values, which are set as a constant for each wavelength and were estimated from the average pixel values (over many observations) of the quiet Sun. The resulting absorption ratios are plotted to give a spatial map of the composition, as seen in the figures in the following section. In addition, the total absorption in Hα and He I, the average He/H absorption ratio, and the root-mean-square (RMS) deviation of the absorption ratio are calculated for the erupting portion of the filament.

The physical meaning of the absorption ratio is that it provides a relative measure of the column density of neutral helium, as compared to the column density of neutral hydrogen, because of how the two lines are formed at $10^4 \; K$. He I 10830 Å is formed by photoexcitation between the lowest triplet states of neutral helium ($1s2l \; ^3S$ and ^3P) at a rate nearly unchanged for typical temperatures in a filament (e.g. Andretta & Jones 1997; Labrosse & Gouttebroze 2001, 2004). Hα is formed in neutral hydrogen by a mix of photoexcitation and collisions between the $n = 2$ and $n = 3$ states, with only a square-root dependence of their population levels on the temperature (e.g. Wiik et al. 1992; Gouttebroze et al. 1993; Heinzel et al. 1994). The amount of absorption in both lines is directly dependent on the electron density, and thus on the column density of the atom that forms the line, with slightly shallower logarithmic slopes for an optically thick filament (compared to one that is optically thin). Note that the opacity of filaments and the effects of Doppler broadening are discussed in detail in § 4. The NLTE models (i.e. spectral

models of a plasma not in local thermodynamic equilibrium; references above) do find some scatter in the relation between density and absorption, because of the range of input parameters, besides density), so the column density can only be estimated to within half an order of magnitude or less in any individual observation of a particular filament. However, comparisons among observations of the same filament are much more accurate since the filament plasma parameters should be consistent, and not subject to random variables.

Therefore, by comparing these spectral lines between different observations or among different parts of a filament in the same observation, meaningful *relative* values of the absorptions can be determined, and thus relative values of the column densities and abundances. Consequently, in the maps of the He/H absorption ratio, a darker pixel means there is a relative helium deficit, compared to the amount of hydrogen, while a brighter pixel indicates a relative helium surplus. In addition, the plots of the total absorption and the absorption ratio only show relative changes over time in the column densities and composition, respectively. The RMS deviation of the pixels' absorption ratio values (from the average absorption ratio) in each observation is calculated to quantify the relative degree of the absorption ratio's spatial uniformity, which we will later relate to a homogenization of the material, and its change over time. While there is some scatter in this measure of the uniformity, a decrease in the RMS deviation is a good indicator of a general normalization of the composition over the whole filament structure.

3. Results

The nineteen filaments analyzed in this study range in their size and shape, and they culminate in a mix of full, partial, and failed eruptions (Table 1). The key finding is that, in all cases, the He/H absorption ratio is relatively uniform (i.e. nearly constant) within the erupting part of the filament, starting at least one full day before the eruption. Additionally,

over the same time period, the filaments are active, with visible small-scale motions and an increase in vertical extent, and the amount of absorption in Hα and He I due to the filament material increases continuously (in most cases) from the time of "activation" up to the initiation of eruption (see definitions in § 1).

A typical example of this behavior is the filament eruption from 2002 July 23, which is a full eruption of a large filament. On July 19, the filament is quiescent, showing a low level of activity and a stable size and shape (see Fig. 1(b); also found in Gilbert et al. 2007a). The distribution of neutral H and He is slightly separated (Fig. 2(b)), with a relative helium deficit along the top and a surplus at the bottom. By July 20, two and a half days before the eruption, the filament has become active, with noticeable movement of the material within, and an apparent increase in vertical extent (Fig. 1(c)). During the period of high activity, the absorption ratio (and implicitly the composition) quickly becomes spatially uniform at approximately the same value throughout the filament (Fig. 2(c)); this effect is evident in the initial decrease of the RMS deviation of the absorption ratio, which then changes little over the next three days (Fig. 3(d)). In addition, the total absorption in Hα and He I increases sharply at the time of this apparent homogenization and continues increasing up to the time of the eruption (Figs. 3(a) and 3(b)). The filament erupts fully on July 23 at 09:00 UT (as observed by EIT), and the resultant CME appears in LASCO/C2 later that day at 19:31. This eruption shows a clear and steady increase in absorption in Hα and He I, but aside from an initial decrease in the RMS deviation, the amount of homogenization in the absorption ratio does not continue increasing throughout the active period.

A comparison of this eruption with the failed eruption on 2004 Aug 11 of a medium-sized filament better illustrates the range of the trends observed. This filament is initially quiescent, and Aug 7 shows clear bands of helium deficit and surplus (Fig. 5(a)). Early on
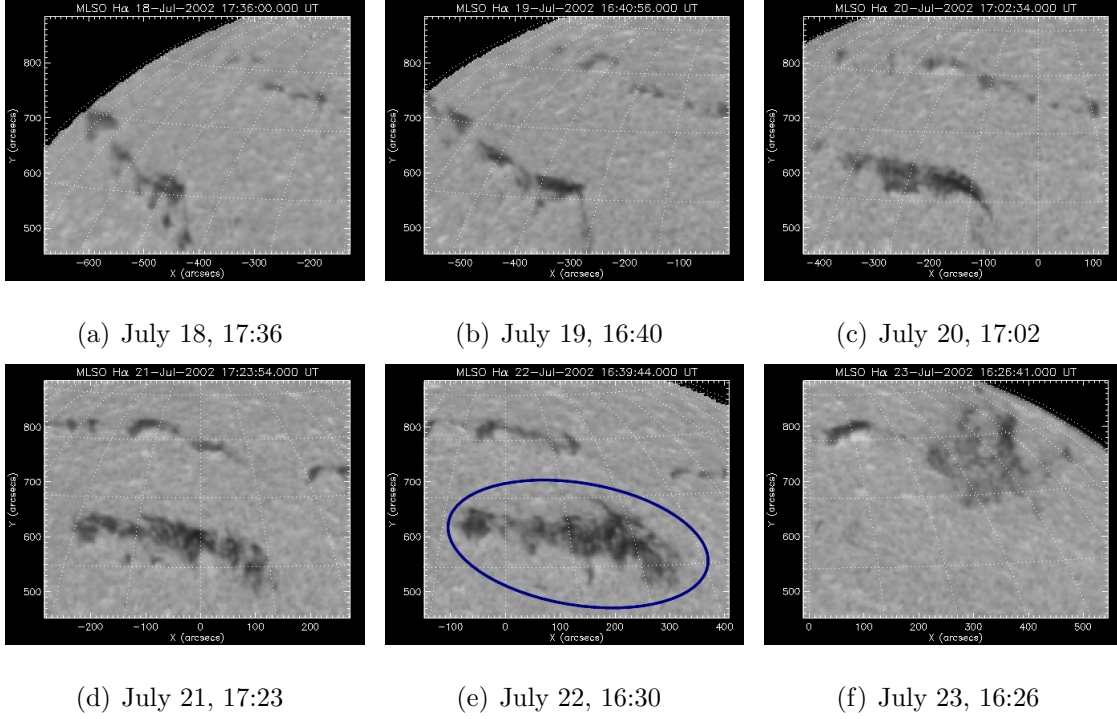
(a) July 18, 17:36   (b) July 19, 16:40   (c) July 20, 17:02

(d) July 21, 17:23   (e) July 22, 16:30   (f) July 23, 16:26

Fig. 1.— Series of MLSO Hα 6563 Å images of a large quiet Sun filament preceding its full eruption on 2002 July 23 at 09:00 UT. The erupting filament is *circled* in (e). All times are UT. [Both the Hα and He I observations are available as mpeg animations in the electronic edition of the Journal.]

(a) July 18, 17:36   (b) July 19, 16:40   (c) July 20, 17:02

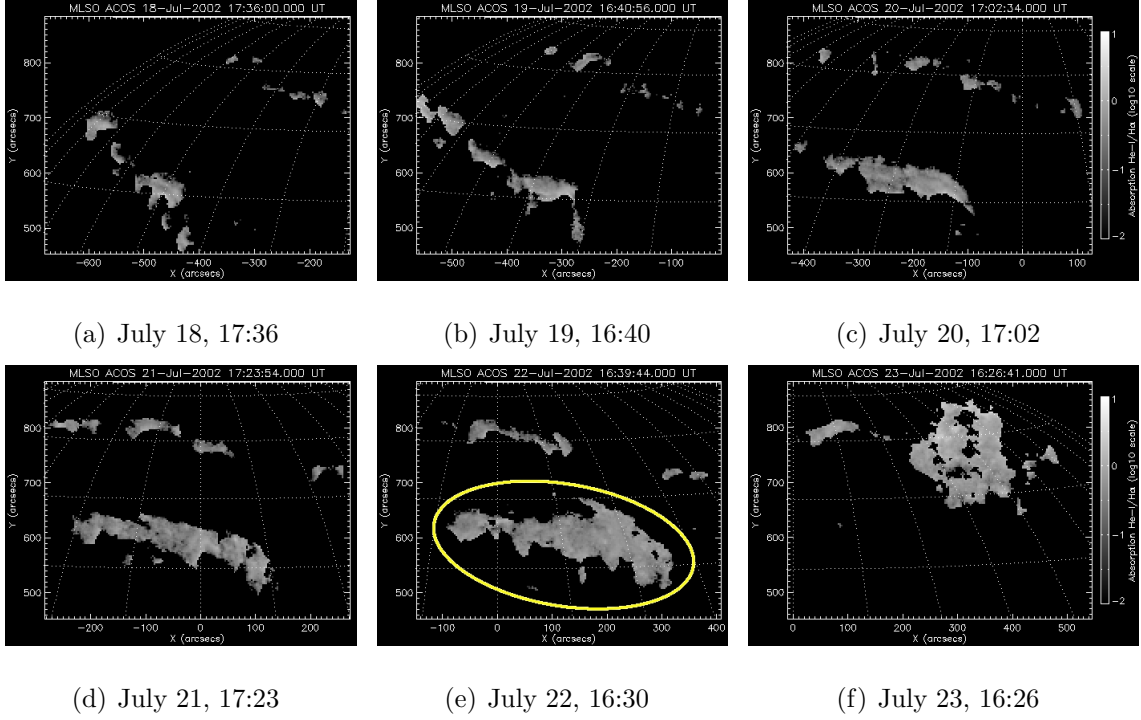(d) July 21, 17:23   (e) July 22, 16:30   (f) July 23, 16:26

Fig. 2.— Series of He/H absorption ratio maps of a large quiet Sun filament that erupts on 2002 July 23 at 09:00 UT. The absorption ratio is plotted on the same log-scale for all maps, where a brighter pixel corresponds to a relative surplus of absorption in He I as compared to Hα, and a darker pixel shows a relative helium deficit. The erupting filament is *circled* in (e). The absorption ratios become more spatially uniform during the nighttime between (b) and (c). All times are UT. [This figure is available as an mpeg animation in the electronic edition of the Journal.]
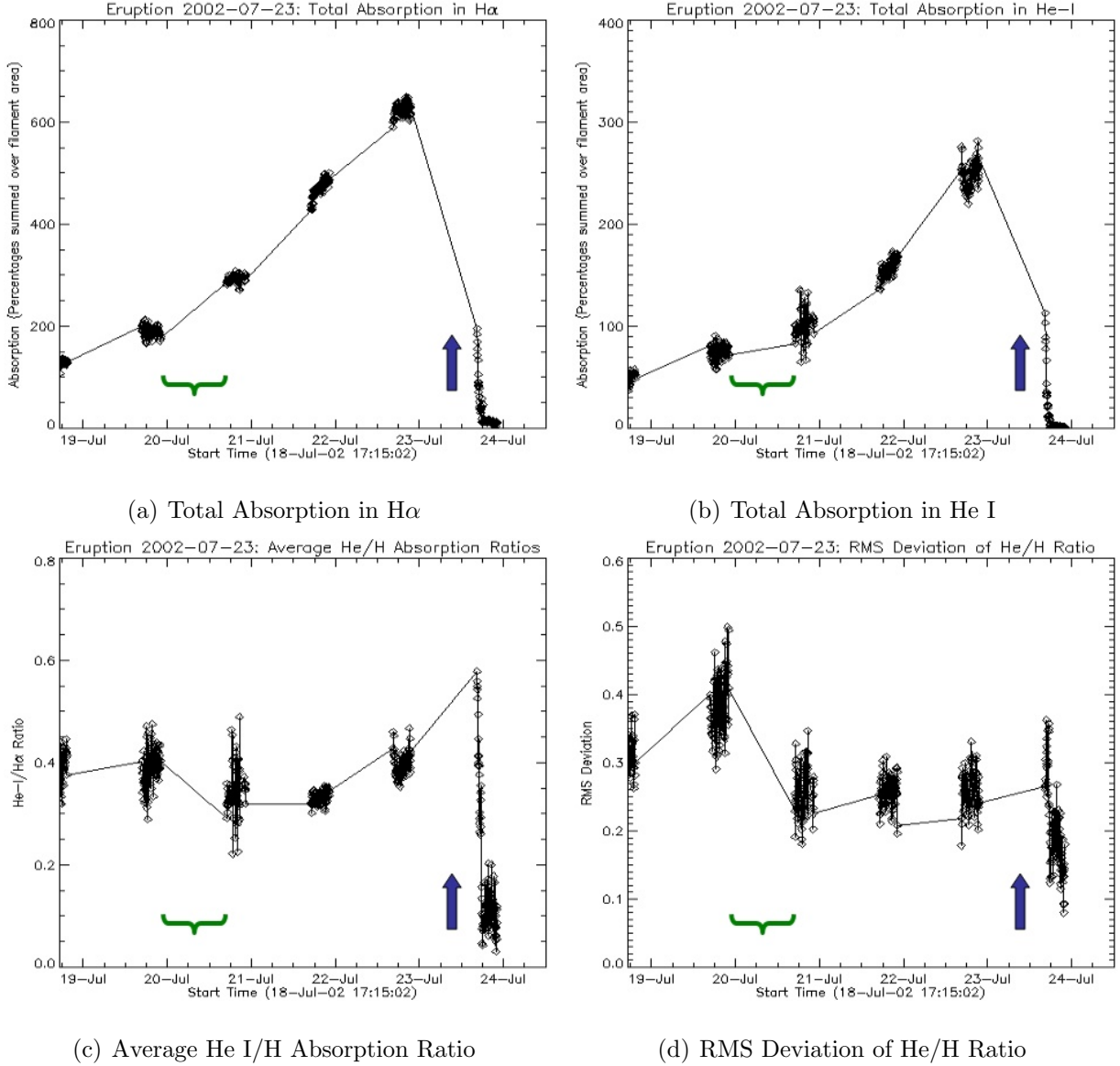
(a) Total Absorption in Hα

(b) Total Absorption in He I

(c) Average He I/H Absorption Ratio

(d) RMS Deviation of He/H Ratio

Fig. 3.— Six-day plots of the total absorption in Hα and He I, the average He/H absorption ratio, and its RMS deviation over the entire filament that erupts on 2002 July 23 at 09:00 UT. The total absorption is the sum of the erupting filament pixels' percentages of absorption for each line. The *brackets* indicate the nighttime during which the absorption ratios become more uniform, and the *arrows* denote the start of the eruption. The daily observing window at MLSO is between 17:00 and 02:00 UT.

Aug 9 there is a small increase in activity, and during Aug 10 the activity greatly increases during the build up to the eruption the next day at 22:15 UT (Fig. 4). The absorption ratios start changing slowly on Aug 9 (soon after Fig. 5(b)), but do not become significantly more uniform until Aug 10 (Fig. 5(d)), as evidenced by the steep decline in the RMS deviation that day (Fig. 6(d)). There is a slow decrease in the RMS deviation from Aug 9 to 10 during a period of slightly higher activity, although this is partially caused by the Sun's rotation since a view from above would not see the vertical stratification of neutral H and He in quiescent filaments (discussed in Gilbert et al. 2007a). The absorption in Hα increases slightly for several days prior to Aug 10 (Fig. 6(a)), and the He I absorption actually decreases (Fig. 6(b)), before a sharp increase in absorption in both lines that is concurrent with the swiftly increasing uniformity of the absorption ratio on Aug 10. Flaring in the nearby active region to the northeast occurs simultaneous to the filament eruption and might be related. However, the EIT cadence is too low to detect any coronal waves, and no direct connection between the active region flaring and the initiation of eruption can be formed from the available data.

EIT observations show the post-eruption filament rising high in the corona, draining its material down apparent magnetic field lines, then resettling with the footpoints and barbs in the same positions. A faint "cavity-like" CME (with a weak leading edge and no discernible inner core) is seen in LASCO on Aug 12 at 06:00. The filament reforms about one day later (Fig. 4(g)), and maintains a high level of activity while again increasing in Hα and He I absorption, concurrent to decreases in the RMS variation. This high activity leads up to another failed eruption on Aug 15 at 01:30 UT, which is quickly contained by overlying field. In summary, this filament shows only slight initial increases in the spatial uniformity and Hα absorption, and a decrease in He I absorption, for the initial two days of low activity, before a sharp increase in activity, apparent homogenization, and absorption in both lines the day before the first eruption. The short period of high activity cannot
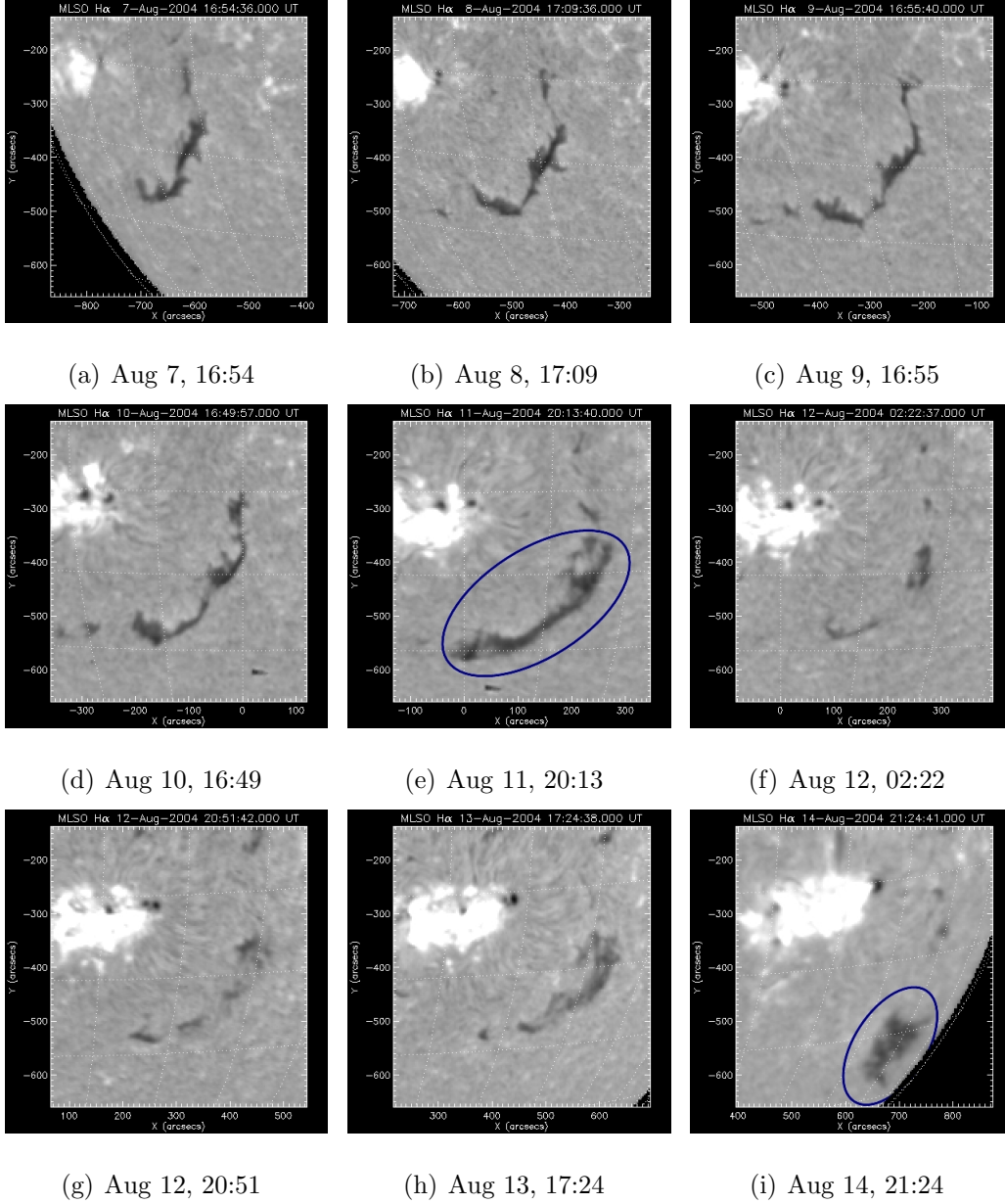
(a) Aug 7, 16:54   (b) Aug 8, 17:09   (c) Aug 9, 16:55

(d) Aug 10, 16:49   (e) Aug 11, 20:13   (f) Aug 12, 02:22

(g) Aug 12, 20:51   (h) Aug 13, 17:24   (i) Aug 14, 21:24

Fig. 4.— Series of MLSO Hα 6563 Å images of a medium-sized quiet Sun filament during its failed eruption on 2004 Aug 11 at 22:15 UT, reformation on Aug 12, and second failed eruption on Aug 15 at 01:30 UT. The erupting filament is *circled* in (e) and (i). All times are UT. [Both the Hα and He I observations are available as mpeg animations in the electronic edition of the Journal.]

(a) Aug 7, 16:54   (b) Aug 8, 16:40   (c) Aug 9, 16:55

(d) Aug 10, 16:49   (e) Aug 11, 20:13   (f) Aug 12, 02:22

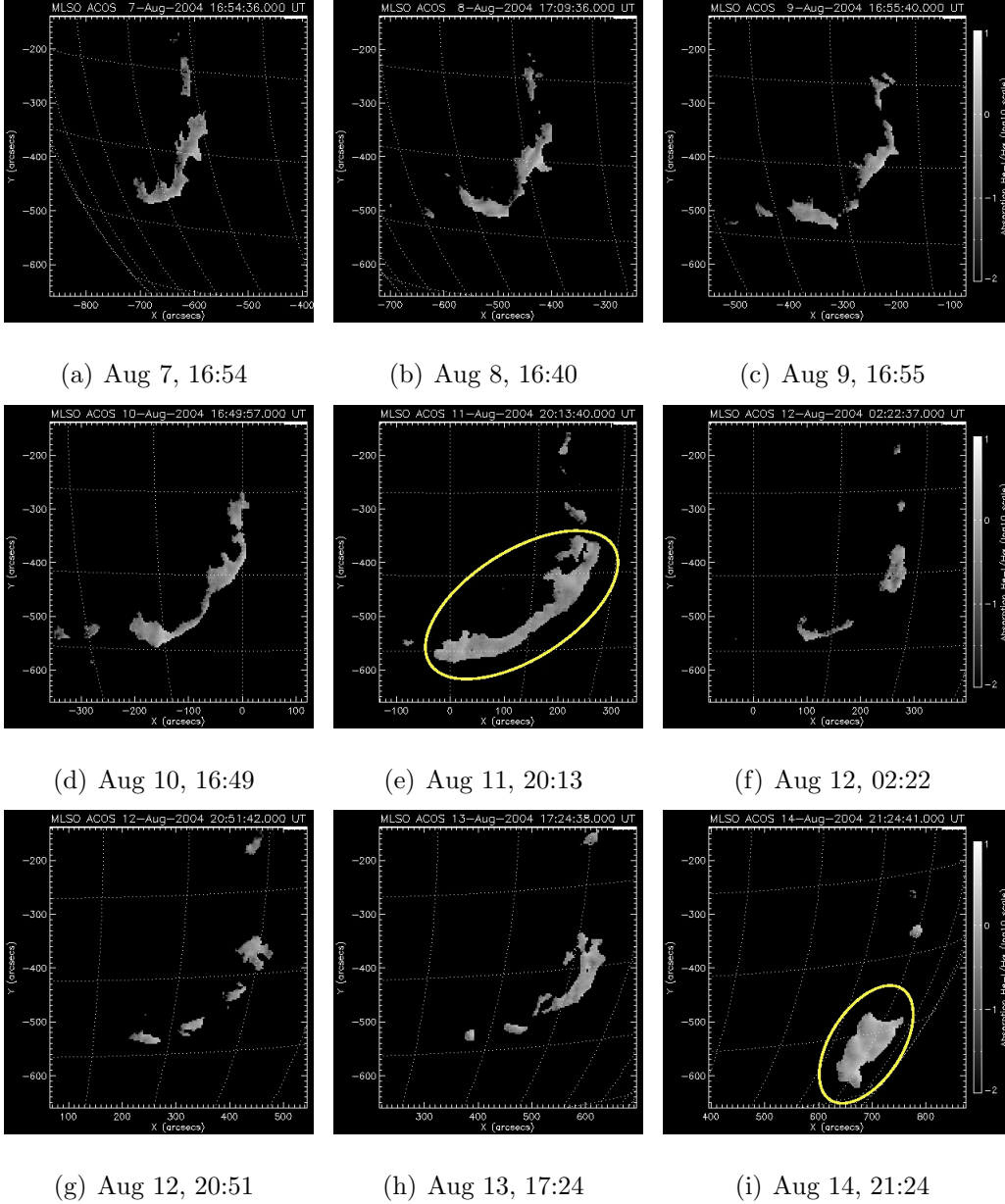(g) Aug 12, 20:51   (h) Aug 13, 17:24   (i) Aug 14, 21:24

Fig. 5.— Series of He/H absorption ratio maps of a medium-sized quiet Sun filament that erupts on 2004 Aug 11 at 22:15 UT, reforms on Aug 12, and erupts again on Aug 15 at 01:30 UT. The absorption ratio is plotted on the same log-scale for all maps, where a brighter pixel corresponds to a relative surplus of absorption in He I as compared to Hα, and a darker pixel shows a relative helium deficit. The erupting filament is *circled* in (e) and (i). The absorption ratios start becoming highly uniform in (d). All times are UT. [This figure is available as an mpeg animation in the electronic edition of the Journal.]
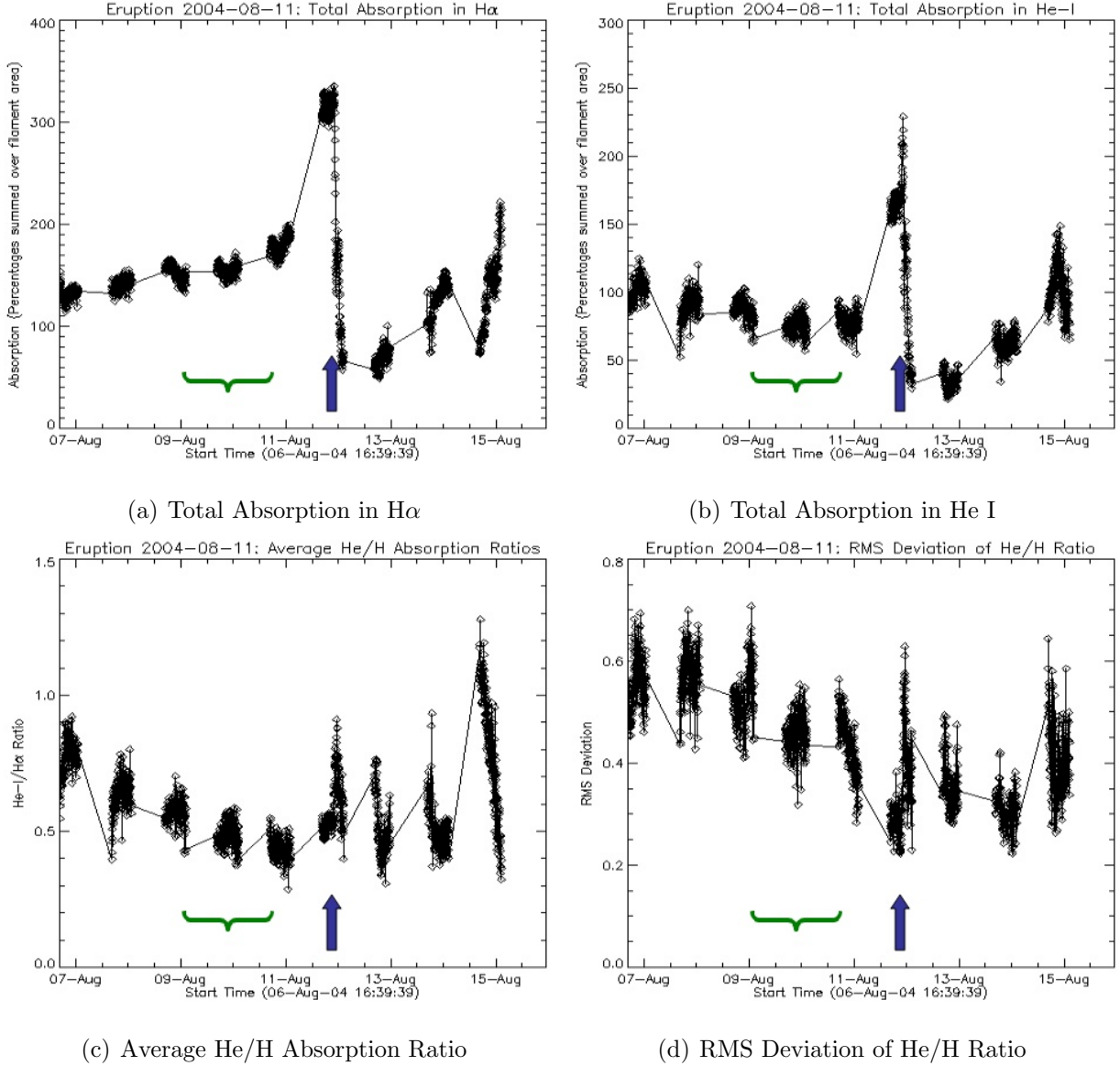
(a) Total Absorption in Hα

(b) Total Absorption in He I

(c) Average He/H Absorption Ratio

(d) RMS Deviation of He/H Ratio

Fig. 6.— Six-day plots of the total absorption in Hα and He I, the average He/H absorption ratio, and its RMS deviation over the entire filament that erupts on 2004 Aug 11 at 22:15 UT, reforms on Aug 12, and erupts again on Aug 15 at 01:30 UT. The total absorption is the sum of the erupting filament pixels' percentages of absorption for each line. The *brackets* indicate the time period of slightly higher activity from Aug 9 to 10, after which the activity greatly increases, and the *arrows* denote the first eruption. The daily observing window at MLSO is between 17:00 and 02:00 UT.

illustrate well the long trend of increasing absorption, but the sharp decline in the RMS deviation during Aug 10 shows the rate of homogenization and its simultaneous start with the increase in absorption at around 20:00 UT. The second eruption provides a more typical example with the start of the observed trends approximately 50 hours prior to eruption initiation, and more gradual changes in the increasing absorptions and spatial uniformity of the absorption ratio.

The combined trends of filament activation, apparent near-homogenization of composition, and increases in absorption all start within about an hour of each other, and at least one day prior to eruption for all nineteen of the filaments considered, regardless of size and type (Fig. 7). The RMS deviation of the absorption ratio decreases monotonically for twelve filaments during the active period, and three others show a decrease after a short initial increase, with the increase occurring simultaneously with a jump in the absorption. Although a high degree of uniformity is clear in the remaining four filaments (2001 Aug 17, 2003 July 11 22:00, 2005 Aug 15, and 2006 June 2, which are all small in size and greatly increase in Hα absorption; see Fig. 7), the value of the RMS deviation increases slightly during the active period. However, these four filaments are quite small and appear to be already homogenized before activation (while they are still forming), and thus they had a relatively low RMS deviation at the start.

Between activation and eruption, the absorption increases in Hα and He I for seventeen of the nineteen filaments, with the exceptions being eruptions of only a small fraction of the material (2004 June 2 and 2005 July 9; see Fig. 7). The smallest filaments show a tendency to erupt the soonest after activation – about two days on average – while the largest filaments erupt no earlier than two days after activation, with an average of about three days (see Table 1). However, the wide spread in these times indicates that size is not a dominant factor in determining the length of time between activation and eruption.
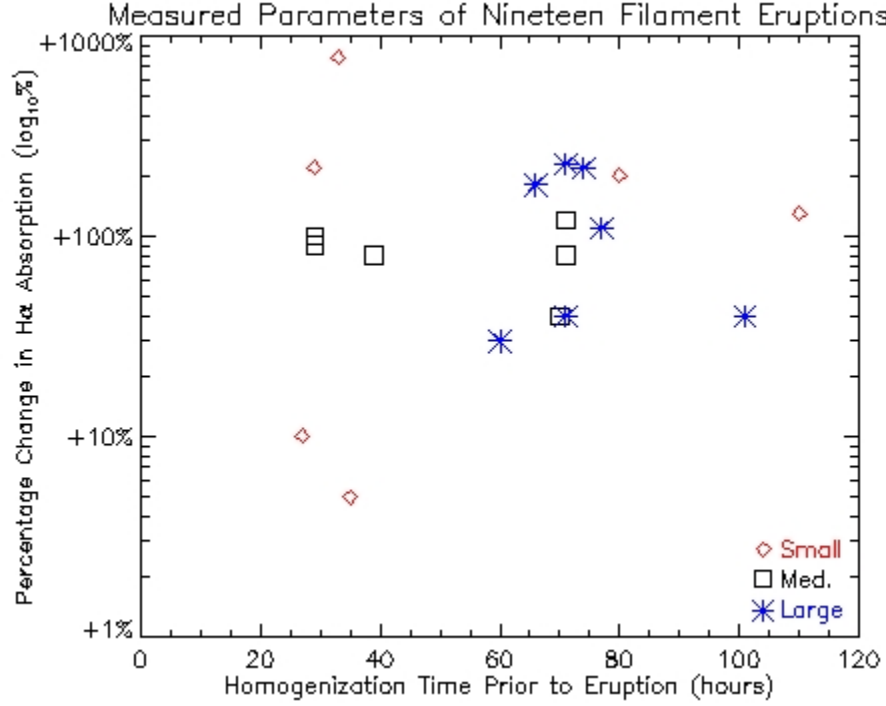
Fig. 7.— Semi-log scatterplot for the nineteen filament eruptions, classified by size, of the percentage increase in the total absorption in Hα versus the number of hours prior to eruption when homogenization of the absorption ratio starts. The total absorption is the sum of the erupting filament pixels' percentages of absorption for each line. Note that the two small filaments in the lower-left erupted only a minor fraction of material, and the other four small filaments exhibited slight increases in the RMS deviation during their active periods.

Table 1. Summary of Filament Eruptions

Event	Date & Time of Eruption (UTC)	Eruption Location (arcsec)[a]	Filament Size	Homogenization Time Prior to Eruption (hr)	Percentage Change in Absorption[b]	Eruption Type	Related CME, Position Angle & Angular Width[c]
1	2000-02-19, 21:00	[150, 750]	Medium	$t \approx 29$	+100%	Partial	00:30, 327°, 88°
2	2000-04-11, 19:30	[600, -600]	Large	$96 > t > 47$	+40%	Partial	20:30, 210°, 45°
3	2001-06-10, 18:00	[250, -550]	Medium	$94 > t > 46$	+120%	Failed	None
4	2001-08-17, 19:00	[-300, 450]	Small	$t > 75$	+200%	Failed	None
5	2002-04-26, 16:45	[100, -550]	Large	$67 > t > 24$	+180%	Partial	18:52, 209°, 96°
6	2002-06-10, 18:55	[150, 450]	Large	$93 > t > 50$	+230%	Failed	None
7	2002-07-23, 09:00	[350, 600]	Large	$83 > t > 64$	+220%	Full	19:31, 319°, 116°
8	2003-06-11, 16:30	[-250, -600]	Large	$t > 72$	+110%	Partial	18:50[d], 150°, 45°
9	2003-07-11, 20:30	[100, -600]	Medium	$t > 67$	+80%	Partial	00:30, 196°, 118°
10	2003-07-11, 22:00	[350, 350]	Small	$t \approx 29$	+220%	Failed	None
11	2004-05-24, 17:20	[-50, 400]	Medium	$t \approx 39$	+80%	Full	21:26, 354°, 131°
12	2004-06-02, 22:20	[-100, 250]	Small	$t \approx 27$	+10%	Failed	None
13	2004-08-11, 22:15	[200, -500]	Medium	$t \approx 29$	+90%	Failed	06:00, 195°, 40°

4. Discussion and Conclusions

The combined observational trend of a high degree of spatial uniformity of the He/H absorption ratio, high level of activity, and increases in Hα and He I absorption, all starting at least one day prior to every eruption considered, is a compelling result. The spatially near-constant ratio suggests that the composition could be quite similar throughout the filament, which is clearly different from the separated distribution of neutral H and He in quiescent filaments, found by Gilbert et al. (2007a). The change from a separated distribution to an apparently near-homogeneous composition may result from a number of causes. The filament material might be mixing as a consequence of dynamic motions that are readily visible in highly active filaments, although then the question shifts to the source of those active motions. Another, perhaps more intriguing idea is that the combined trend is a result of mass loading into the filament, in which the newly loaded material mixes and overwhelms the previous, quiescent distribution of H and He. This possibility would directly explain the large absorption increases observed simultaneously in Hα and He I, in addition to the concurrent high level of activity. However, before settling on a specific physical mechanism, we must be careful to consider other factors that can affect the measured absorptions and the absorption ratio, aside from the column densities.

The variable optical thickness in filaments complicates the interpretation of these observations, as there are often both optically thick and thin regions in the same filament section (in these lines, opacity $\tau \sim 1$). This mix of opacity, combined with the potentially significant effects of Doppler broadening, can deceptively affect the absorption measured by an instrument. An optically thin profile that is Doppler-broadened will decrease in absorption since some material will shift outside of the instrument's bandpass. However, an optically thick profile is saturated at line center, so when it is Doppler broadened, the amount of absorption measured by the instrument will increase as the line profile fills

Table 1—Continued

Event	Date & Time of Eruption (UTC)	Eruption Location (arcsec)[a]	Filament Size	Homogenization Time Prior to Eruption (hr)	Percentage Change in Absorption[b]	Eruption Type	Related CME, Position Angle & Angular Width[c]
14	2004-12-24, 04:15	[250, 800]	Large	$t \approx 101$	+40%	Full	05:36, 291°, 92°
15	2005-06-07, 09:00	[-350, 450]	Medium	$t > 65$	+40%	Full	10:24, 65°, 77°
16	2005-07-09, 20:40	[-500, 550]	Small	$43 > t > 28$	+5%	Partial	21:54, 75°, 62°
17	2005-08-15, 17:50	[-300, -550]	Small	$42 > t > 25$	+780%	Full	23:54, 117°, 78°
18	2005-09-06, 10:00	[450, 400]	Large	$t \approx 60$	+30%	Full	21:12, 289°, 55°
19	2006-06-02, 03:00	[400, -550]	Small	$115 > t > 106$	+130%	Full	04:24, 246°, 42°

[a] Arcseconds from disk center.

[b] Change during active period of the total Hα absorption, which is the sum of the pixels' percentages of absorption.

[c] From the CDAW SOHO/LASCO CME catalog.

[d] Observed by the MLSO/Mk4 coronagraph.

a greater percentage of the bandpass. For the filaments analyzed here, the line-of-sight (primarily radial) velocities prior to the initiation of the eruptions appear to be small, and there is only a weak signal in MLSO He I velocity data. In addition, this absorption increase occurs simultaneously and to similar degrees in both Hα and He I (Figs. 3 and 6), despite the different instrument bandpasses (and Doppler widths; see § 2). Note that the higher lateral velocity of the material (in counter-streaming flows along the spine) is projected only fractionally onto the line-of-sight, since most of the filaments are either polar-crown or near disk center. Also, in order for the Doppler broadening effect to cause the absorption to increase continually during the period of high filament activity, which occurs in most, but not all of these filaments, then the line-of-sight velocities should be increasing (to some degree) that entire time.

It appears that Doppler broadening might have only a minor effect here, but from this data set we cannot truly pass judgment since the line-of-sight velocities are not measured, so absorption increases related to higher column density are entangled with the effect of Doppler broadening. A future study that includes quantitative Dopplergrams, to measure the line-of-sight velocities, or a combination of multiple Hα and He I instruments with contrasting bandpasses and resolution, would help to separate out the Doppler broadening effect and give better measurements of any increases in the H and He column densities or changes in the composition. Additionally, an NLTE spectral model might be specifically designed to simulate the increased activity, Doppler broadening, opacity, and possible heating prior to eruptions in order to more clearly show how the spectral distribution changes (including or excluding mass increases), and how the measured absorption in Hα and He I and the He/H absorption ratio would change.

A few other notable factors could be affecting the data. Current NLTE models show that an increase in a chromospheric plasma's temperature would increase the absorption,

without any change in the density. However, the large absorption increases observed here mean that the average temperature would need to increase much higher than is expected in filaments (recall § 2, and see discussion in Kucera & Landi 2008). Conversely, filament material initially at transition region temperatures could cause more absorption in Hα and He I as it cools to chromospheric temperatures. Thirdly, a change in perspective or a shift of the filament structure could modify the column density without an actual density increase, although high activity in this sample of filaments is not associated with large-scale motion of the spine, and the variety of positions on the solar disk rules out solar rotation as a possible cause. Finally, the filaments' range of sizes, shapes, locations relative to active regions, positions on the solar disk, and eruption types mean that these five factors are unlikely to be significantly affecting the results or causing the observed trend.

Although these caveats hinder the certainty of any conclusion, an extended period of mass loading prior to eruption is plausible as an explanation for the combined four-part trend that we observe. A full test of a pre-eruption mass loading scenario would need to include several sequential measurements of the filament mass (e.g. by analyzing sequential high temperature EUV observations; Kilper 2009), along with a comparison of the measured rate of mass increase to theoretical rates from various mass loading models, such as chromospheric evaporation (Antiochos & Klimchuk 1991). Going further, a future study of the timing among various precursors to eruption that have been observed – including homogenization of composition, increases in absorption, increases in cavity size, heating before and during, and sometimes flux emergence (references in § 1) – would significantly advance the understanding of the physical mechanism driving the eruptions.

The need to compare the various eruption models (e.g. Moore et al. 2001; Low et al. 2003) to observations and the general importance of solar eruptions will motivate continued research in this area. Prospects for further progress are bright with the new fleet of

observatories – especially the STEREO spacecraft, which provide two more vantage points for observations during the build up to eruptions of filaments, making it possible to compare the timing among the various observational precursors to eruption.

As a final remark, the day or more of lead time between the apparent homogenization of the He/H absorption ratio and the eruption suggests that our method, in principle, could be used to predict when and where a filament eruption may occur. A real-time analysis of co-temporal neutral H and He observations could be implemented with minimal user interaction to assist space weather forecasters and also observers that wish to capture an eruption with their instruments. However, there are two main caveats that currently limit the effectiveness of such an approach. The spatial homogenization is also observed to occur in many non-erupting filaments, especially those that are forming or increasing in size (Kilper 2009), making any prediction very uncertain, although a systematic study of varying filaments and a refinement of the method should improve the predictive capability. Secondly, the large spread in the amount of time between the start of homogenization and the actual initiation of eruption observed in this study (even when the eruptions are grouped by size) means that it would be difficult to pinpoint the time of eruption much in advance. Indeed, the method of a real-time analysis of the He/H absorption ratio is more suited for determining when eruptions will *not* occur, allowing advanced forecasting of "All Clear" periods when space weather conditions will be safe, instead of when there is imminent danger.

Facilities: HAO, SOHO.

REFERENCES

Alexander, D. 2006, Space Sci. Rev., 123, 81

Andretta, V., & Jones, H. P. 1997, ApJ, 489, 375

Antiochos, S. K., & Klimchuk, J. A. 1991, ApJ, 378, 372

Cirigliano, D., Vial, J.-C., & Rovira, M. 2004, Sol. Phys., 223, 95

Elmore, D. F., et al. 1998, Appl. Opt., 37, 4270

Engvold, O., Jakobsson, H., Tandberg-Hanssen, E., Gurman, J. B., & Moses, D. 2001, Sol. Phys., 202, 293

Feynman, J., & Ruzmaikin, A. 2004, Sol. Phys., 219, 301

Fisher, R. R., Lee, R. H., MacQueen, R. M., & Poland, A. I. 1981, Appl. Opt., 20, 1094

Gaizauskas, V., Zirker, J. B., Sweetland, C., & Kovacs, A. 1997, ApJ, 479, 448

Gibson, S. E., Foster, D., Burkepile, J., de Toma, G., & Stanger, A. 2006, ApJ, 641, 590

Gilbert, H. R., Hansteen, V. H., & Holzer, T. E. 2002, ApJ, 577, 464

Gilbert, H., Kilper, G., & Alexander, D. 2007a, ApJ, 671, 978

Gilbert, H., Alexander, D., & Lui, R. 2007b, Sol. Phys., 245, 287

Gouttebroze, P., Heinzel, P., & Vial, J.-C. 1993, A&AS, 99, 513

Heinzel, P., Gouttebroze, P., & Vial, J.-C. 1994, A&A, 292, 656

Kilper, G. 2009, Doctoral thesis, Rice Univ.

Klimchuk, J. A. 2001, in Space Weather, ed. P. Song, H. J. Singer, & G. L. Siscoe (Geophys. Monogr. 125; Washington: AGU), 143

Kopp, G. A., Derks, M. J., Elmore, D. F., Hassler, D. M., Woods, J. C., Streete, J. L., & Blankner, J. G. 1997, Appl. Opt., 36, 291

Kucera, T. A., & Landi, E. 2006, ApJ, 645, 1525

Kucera, T. A., & Landi, E. 2008, ApJ, 673, 611

Labrosse, N., & Gouttebroze, P. 2001, A&A, 380, 323

Labrosse, N., & Gouttebroze, P. 2004, ApJ, 617, 614

Martin, S. F. 1998, Sol. Phys., 182, 107

Moore, R. L., Sterling, A. C., Hudson, H. S., & Lemen, J. R. 2001, ApJ, 552, 833

Low, B. C., Fong, B., & Fan, Y. 2003, ApJ, 594, 1060

Sterling, A. C., & Moore, R. L. 2001, ApJ, 561, L219

Sterling, A. C., Harra, L. K., & Moore, R. L. 2007, ApJ, 669, 1359

Tandberg-Hanssen, E. 1995, The Nature of Solar Prominences, (Dordrecht; Boston: Kluwer)

Wiik, J. E., Heinzel, P., & Schmieder, B. 1992, A&A, 260, 419

Zhang, Y., Zhang, M., & Zhang, H. 2008, Sol. Phys., 250, 75